



Research
Glycomedicine—Article

A Comparative Mechanistic Study of Live-Cell Glycocalyx Engineering: Improving Adoptive Cell Therapies Against B Lymphoma



Yuxin Li^{a,#}, Tao Gao^{a,#}, Zhaoxin Han^a, Valeria M. Stepanova^b, Han Wang^a, Hongmin Chen^a, Alexey Stepanov^{b,c}, Senlian Hong^{a,*}

^a State Key Laboratory of Natural and Biomimetic Drugs & Chemical Biology Center & Department of Chemical Biology, School of Pharmaceutical Sciences, Peking University, Beijing 100191, China

^b Shemyakin-Ovchinnikov Institute of Bioorganic Chemistry, Russian Academy of Sciences, Moscow 117997, Russia

^c Department of Integrative Structural and Computational Biology, The Scripps Research Institute, La Jolla, CA 92037, USA

ARTICLE INFO

Article history:

Received 21 April 2025

Revised 8 August 2025

Accepted 28 August 2025

Available online 4 September 2025

Keywords:

Glycocalyx

Live-cell engineering

Adoptive immunotherapy

Glycoproteomics

B lymphoma

ABSTRACT

Adoptive cell therapies (ACTs) have achieved remarkable clinical success in treating cancers; however, their broader application is greatly impeded by high cost and restricted antigen specificity. Recently, engineering the glycocalyx has provided a convenient transgene-free means to design ACTs with high-avidity glycan ligands to target CD22, offering a new avenue for B lymphoma immunotherapy. In this work, we perform a comparative analysis of the molecular profiles involved in metabolic or chemoenzymatic glycocalyx engineering and explore their multiplexing capability. The glycoproteomic results revealed content-dependent customization of the natural killer (NK)-92MI glycocalyx. Compared with metabolic engineering, exogenous chemoenzymatic engineering has comparable or even superior ligand-loading efficiency, with some immune synapse components modified to facilitate their spatial recognition against target cells. Next, we tested the orthogonal creation of ligands on NK-92MI cells by further engineering α 2,3-sialylated *N*-acetylglucosamine moieties to produce selectin ligands that are essential for better *in vivo* eradication of mouse xenograft B lymphoma. Finally, we demonstrate that analogous engineering of CD19-targeted chimeric antigen receptor T (CAR-T) cells to produce CD19/CD22 bitargeted therapy can enhance antigen targeting and tumor cell killing, offering an alternative cost-efficient agent for treating cancer relapse with decreased levels of CD19 antigens. These findings establish a mechanistic foundation for glycocalyx engineering and support the rational design of next-generation ACTs against B lymphoma.

© 2025 THE AUTHORS. Published by Elsevier LTD on behalf of Chinese Academy of Engineering and Higher Education Press Limited Company. This is an open access article under the CC BY-NC-ND license (<http://creativecommons.org/licenses/by-nc-nd/4.0/>).

1. Introduction

B lymphoma is the most frequent type of hematolymphoid tumor. The emergence of adoptive cell therapy (ACT), particularly CD19-specific chimeric antigen receptor T (CAR-T) cells, has revolutionized the patient care paradigm [1,2]. These cost-ineffective cellular immunotherapies leverage naturally occurring or engineered immune killers, such as natural killer (NK) and cytotoxic T cells, to recognize and destroy B lymphoma [3,4]. Unfortunately, intrinsic challenges remain in their clinical application. Intensive attempts to optimize ACT functional persistence in the tumor

microenvironment (TME) have led to a comprehensive understanding of effector immune responses, including their inherent cytotoxicity against target cells, antigen sensitivity, tumor infiltration capacity, hypofunctional transformation, and suppressive circuits [5]. Converging immune cell biology and genetic/nongenetic engineering tools to improve ACT effector responses against cancers represents an emerging research field [6].

In addition to the well-known CD19, CD22 is another critical therapeutic antigen for B lymphoma and belongs to the sialic acid (Sia)-binding immunoglobulin-like lectin (Siglec) family [7,8]. Both antibody and CAR-T therapies targeting CD22 are currently under intensive clinical investigation [8,9]. Among the treatments, TriCAR-acute lymphoblastic leukemia (ALL) T-cells, which are designed to target CD19, CD20, and CD22, bring renewed hope to patients with relapsed or refractory B-cell lymphoma [10].

* Corresponding author.

E-mail address: hongsen414@pku.edu.cn (S. Hong).

These authors contributed equally to this work.

Moreover, several researchers have screened high-avidity ligands derived from Sia analogs to target CD22 [11]. Examples include 9-*N*-*m*-phenoxybenzamide-*N*-acetylneuraminic acid (^{MPB}Neu5Ac) and 9-*N*-biphenyl carboxamide-Neu5Ac (^{BPC}Neu5Ac), both of which feature substituents at the C9 position with selective affinities for CD22 in the micromolar range [12]. In addition, paucivalent ligands demonstrate significantly higher avidity (up to 1500-fold) than monovalent ligands do, offering cost-effective alternatives to traditional antibodies [13]. Despite these advances, therapies using antibodies or paucivalent ligands are still associated with serious on-target/off-disease side effects [14,15]. Recently, Wang et al. [16] cultured NK-92 cells with ^{MPB}Neu5Ac, providing this off-the-shelf therapy with the ability to target CD22 after metabolic incorporation. They reported that the injection of ^{MPB}Neu5Ac-modified NK-92 cells improved the growth control of B lymphoma. In brief, Hong et al. [17] developed a chemoenzymatic strategy to modify NK-92MI cells with ^{BPC}Neu5Ac, effectively targeting NK-92MI cells to treat B lymphoma. Importantly, these Sia-ligand-armed NK therapies leverage their inherent immune discrimination for non-self invaders while leaving self-cells untouched, making them a viable option despite their limited efficacy in the intravenous adoptive treatment of B lymphoma. By combining biorthogonal chemistry, glycocalyx engineering facilitates a convenient upload of various agencies to customize anticancer responses, such as targeting multiple antigens or improving TME trafficking [18–23]. Given that glycans are structurally diverse molecules involved in many biological processes [24–26], we believe that in-depth insight into sialylated glycan profiles could significantly broaden the applications of this technology to create cellular immunotherapies with the desired properties.

To this end, we characterized the molecular details of the NK-92MI cells that define the functionality-loading efficiency of metabolic glycocalyx engineering (MGE) of sialylated glycans and chemoenzymatic glycocalyx engineering (CeGE) mediated by β -galactoside α 2,6 sialyltransferase 1 (ST6Gal1). Subsequently, the functionality-loading capacity for the MGE approach was probed with the newly developed unnatural sugar 1,6-di-*O*-propionyl-*N*-azidoacetylmannosamine (1,6Pr₂ManNAz), and the accessibility of the ST6Gal1-assisted CeGE was elucidated by an azide-bearing substrate (Fig. 1(a)). The corresponding glycoproteins were subsequently enriched and identified by mass spectrometry. Proteomic analysis further aligned the promise of ST6Gal1-based engineering of NK-92MI cells with supervisory loading efficiency and coverage for immune synapse components that might facilitate the engaging and killing of B lymphoma by NK-92MI cells. We also assessed the orthogonality of the ST6Gal1-assisted incorporation of ^{MPB}Neu5Ac for CD22 targeting with the *in situ* generation of selectin ligands by exogenous α 1,3-fucosylation. In a murine xenograft tumor model, increased levels of selectin ligands were essential for the *in vivo* control of tumor growth by ^{MPB}Neu5Ac-armed NK-92MI cells. In addition, the incorporation of ^{MPB}Neu5Ac onto CD19-CAR-T cells can similarly enhance their targeting and killing of CD22-positive malignancies. These findings establish the use of live-cell glycocalyx engineering as a versatile strategy to refine cellular immunotherapies and overcome barriers in cancer treatment.

2. Materials and methods

2.1. Reagents

Antibiotin-horseradish peroxidase (HRP) was purchased from Cell Signal Technology (USA). Alkyne-polyethylene glycol (PEG)₄-cyanine 5 (Cy5), alkyne-PEG₄-biotin, water-soluble dibenzo-cyclooctyne (DBCO)-biotin, and water-soluble DBCO-

Cy5 were purchased from Click Chemistry Tools (USA). Cytidine monophosphate-*N*-azidoacetylneuraminic acid (CMP-Neu5Az) and guanosine-5'-diphosphate- β -*L*-fucose (GDP-Fuc) were purchased from Shanghai Biochemsyn (China). Celltracker Deep Red and Celltracker 5-chloromethylfluorescein diacetate (CMFDA) were obtained from Thermo Fisher Scientific (USA). The lactate dehydrogenase (LDH) detection kit was from Promega (USA). *Aleuria aurantia* lectin (AAL)-biotin, *Sambucus nigra* lectin (SNA)-biotin, and *Maackia amurensis* lectin II (MAL-II)-biotin were purchased from VectorLabs (USA). Fluorescein isothiocyanate (FITC)-conjugated anti-human/mouse cutaneous lymphocyte antigen (CLA), anti-human CD19, and anti-human CD22 antibodies were obtained from Biolegend (USA). Streptavidin-Alexa Fluor 647 was purchased from Invitrogen (USA). FITC-conjugated anti-human immunoglobulin G (IgG) antibody was purchased from Abcam (USA). CD22-fragment crystallizable (Fc) was obtained from Sinobiological (China). An inferno- γ (IFN- γ) enzyme linked immunosorbent assay (ELISA) kit was purchased from Solarbio (China).

2.2. Cell culture

Daudi, Raji, Jurkat, BJAB, Ramos, HEK293-FT, and NK-92MI cells were obtained from the laboratory of Dr. Xing Chen (Peking University, China). GM12878 was purchased from the BeNa Culture Collection (China). A Raji cell line stably expressing firefly luciferase and tdTomato (Raji-Luc) was established by lentiviral infection. Daudi, Raji, Jurkat, BJAB, GM12878, and Ramos cells were kept in Roswell Park Memorial Institute (RPMI)-1640 media (Gibco, USA) supplemented with 10% fetal bovine serum (FBS; Gibco), 100 U·mL⁻¹ penicillin G (Gibco), and 100 μ g·mL⁻¹ streptomycin (Gibco). HEK293-FT cells were cultured in high-glucose complete Dulbecco's modified Eagle's medium (DMEM) containing 10% FBS, 100 U·mL⁻¹ penicillin G, and 100 μ g·mL⁻¹ streptomycin. NK-92MI cells were cultured in α -minimal essential medium (α MEM) supplemented with 12.5% FBS, 12.5% horse serum, 0.2 mmol·L⁻¹ inositol, 0.1 mmol·L⁻¹ 2-mercaptoethanol, 0.02 mmol·L⁻¹ folic acid, 100 U·mL⁻¹ penicillin G, and 100 μ g·mL⁻¹ streptomycin. All the cells were cultured in a water-saturated 5% CO₂ incubator at 37 °C.

2.3. Glycocalyx engineering method

1,6Pr₂ManNAz, per-*O*-acetylated *N*-azidoacetylmannosamine (Ac₄ManNAz), ^{MPB}Neu5Ac, and CMP-^{MPB}Neu5Ac were synthesized as previously reported [27–29]. ST6Gal1 was purified following established protocols [30]. For CeGE, the cultured cells were washed twice using phosphate-buffered saline (PBS) and resuspended at a concentration of 1×10^7 cells·mL⁻¹ in labeling buffer (Hanks' balanced salt solution (HBSS) with 3 mmol·L⁻¹ 4-(2-hydroxyethyl)-1-piperazineethanesulfonic acid (HEPES) and 20 mmol·L⁻¹ MgSO₄) supplemented with 40 μ g·mL⁻¹ enzymes and various concentrations of nucleotide sugar donors. After incubation at 37 °C for 30 min, the cells were washed twice with PBS and used for subsequent detection. For MGE, the cells were cultured with probes (1,6Pr₂ManNAz, Ac₄ManNAz, or ^{MPB}Neu5Ac) at different time points, then washed twice with PBS and used for subsequent detection.

2.4. Proteomics sample preparation

For the CeGE group, biotin-labeled cells were washed three times with PBS and lysed with radioimmunoprecipitation assay (RIPA) lysis buffer containing a protease inhibitor cocktail. For the MGE group, azide-labeled cells were washed three times with PBS and lysed with RIPA lysis buffer containing a protease inhibitor

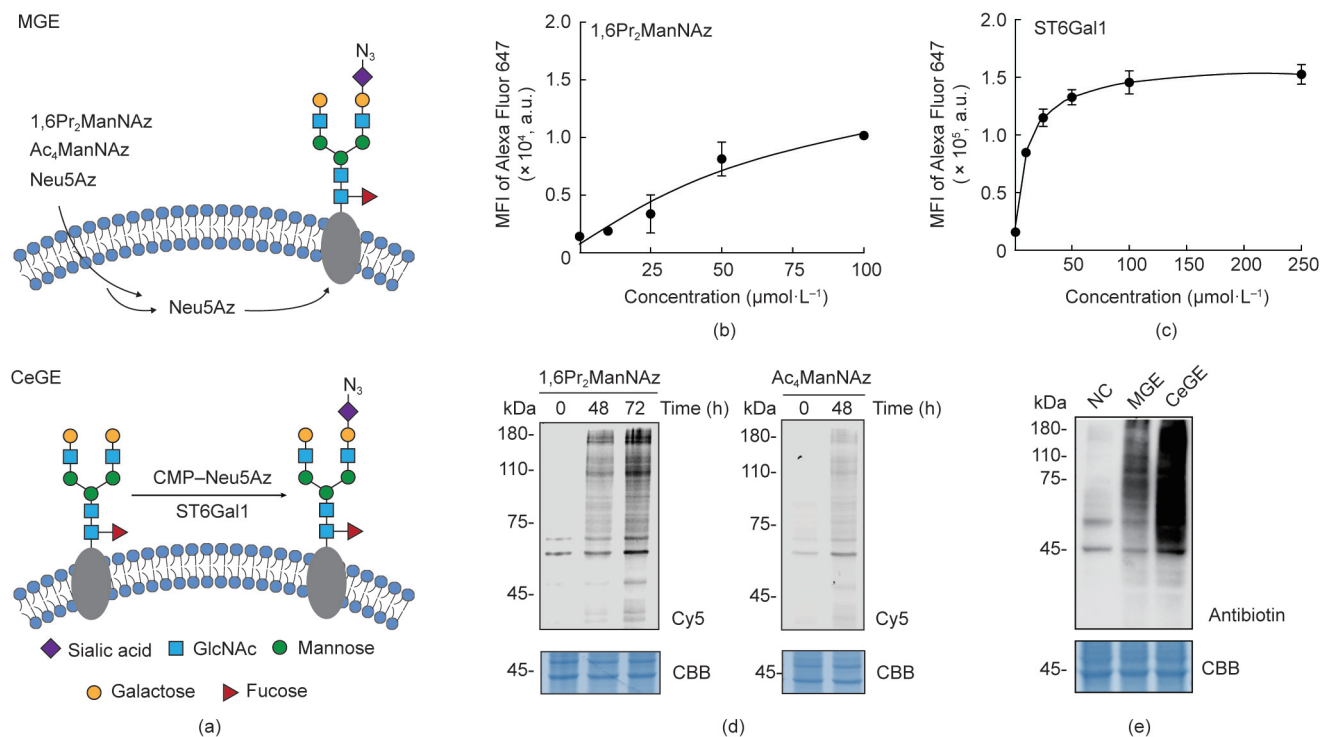


Fig. 1. Engineering the glycocalyx of NK-92MI cells via MGE and ST6Gal1-assisted CeGE. (a) Schematic of glycocalyx engineering-based incorporation of azide-bearing Sia onto surface glycans. (b) Quantification of the 1,6Pr₂ManNAz-assisted MGE labeling of NK-92MI cells by flow cytometry. (c) Quantification of the ST6Gal1-assisted CeGE labeling of NK-92MI cells by flow cytometry. (d) Time-dependent MGE labeling of NK-92MI cells with 1,6Pr₂ManNAz or Ac₄ManNAz. Equal loading was confirmed by Coomassie brilliant blue staining (CBB). (e) Comparison of the labeling efficiency in MGE- and CeGE-treated NK-92MI cells. The error bars in (b) and (c) are expressed as the mean ± standard deviation (s.d.), $n = 3$. Ac₄ManNAz: per-*O*-acetylated *N*-azidoacetylmannosamine; Neu5Az: *N*-azidoacetylneuraminic acid; CMP: cytidine monophosphate; Cy5: cyanine 5; GlcNAc: *N*-acetylglucosamine; NC: negative control; MFI: mean fluorescence intensity; a.u.: arbitrary unit.

cocktail. The resulting protein lysates were quantified using a BCA kit (Thermo Fisher Scientific). The MGE proteins were then tagged with biotin via click chemistry. Biotinylated proteins were isolated by incubation with avidin-agarose beads (Thermo Fisher Scientific) at 4 °C for 4 h. The beads were subsequently washed three times with PBS and once with PBS containing 2% sodium dodecyl sulphate (SDS), followed by resuspension in 200 μL of 8 mol·L⁻¹ urea buffer (100 mmol·L⁻¹ Tris-HCl, pH 8.5). The proteins were reduced with 10 μL of 100 mmol·L⁻¹ tris(2-carboxyethyl)phosphine (TCEP) for 20 min and alkylated with 5 μL of 400 mmol·L⁻¹ iodoacetamide (IAA) for 30 min in the dark. The reaction was quenched with 585 μL of 100 mmol·L⁻¹ Tris-HCl (pH 8.5). After the supernatant was discarded, the proteins on the beads were trypsinized overnight at 37 °C in 200 μL of 2 mol·L⁻¹ urea, 100 mmol·L⁻¹ Tris-HCl (pH 8.5), 2 μL of 100 mmol·L⁻¹ CaCl₂, and trypsin (1:25 ratio to total protein). The supernatant was collected, and the beads were washed twice with 100 mmol·L⁻¹ Tris-HCl (pH 8.5). All the supernatants were combined, and the digestion was stopped with 5% formic acid.

2.5. Mass spectrometry

Peptides were pressure-loaded onto a 250 μm capillary column packed with 2 cm of 10 μm Jupiter C18-A material and 2 cm of a 5 μm Partisphere strong cation exchanger. The buffer solutions used were 5% acetonitrile/0.1% formic acid (Buffer A), 80% acetonitrile/0.1% formic acid (Buffer B), and 500 mmol·L⁻¹ ammonium acetate/5% acetonitrile/0.1% formic acid (Buffer C). The column was subsequently washed with Buffer A. A 100 μm capillary with a 5 μm pulled tip packed with 15 cm of 4 μm Jupiter C18 material was attached via a union, and the assembly was connected to an Agilent 1100 quaternary high-performance liquid chromatography

(HPLC; USA). Peptides were separated using a modified four step gradient: Step 1 (0–100% Buffer B over 90 min), Step 2 (20% Buffer C, 0–100% Buffer B over 100 min), Steps 3–9 (X% Buffer C, 0–100% Buffer B over 110 min, with $X = 30\%–100\%$), and the final step (90% Buffer C, 0–100% Buffer B over 100 min). Peptides were electrosprayed into an Orbitrap Elite mass spectrometer (2.4 kV spray voltage; USA) and analyzed using a cycle of one full-scan Fourier-transform (FT) mass spectrum (300–1600 m/z , 240 000 resolution) followed by 20 data-dependent tandem mass spectrometry (MS/MS) spectra (35% collision energy).

2.6. Mass data analysis

MS/MS spectra were extracted from the XCalibur data system format (.RAW) files using RAW_Xtractor [31] and searched with ProLuCID [32] against a UniProt human database concatenated with a decoy database [33]. Searches were performed on a 100 central processing unit (CPU) Beowulf cluster with no enzyme specificity. Static cysteine modification (57.02146) was included. ProLuCID results were filtered using DTASelect 2.0 [34], and linear discriminant analysis was applied to achieve a protein-level false discovery rate (FDR) < 1% and peptide-level FDR < 1%. Peptides were required to be partially tryptic with < 5 parts per million (ppm) mass deviation. Gene Ontology (GO) and Kyoto Encyclopedia of Genes and Genomes (KEGG) analyses were conducted using the DAVID tool with default parameters.

2.7. CD19-CAR-T cell preparation

For lentiviral production, HEK293-FT cells were transfected with a plasmid encoding CD19-CAR together with packaging and

envelope vectors (pMDLg/pRRE, pMD2.G, and pRSV-Rev) using polyethylenimine (PEI). The culture supernatant was collected at 48 h post-transfection and concentrated by ultracentrifugation before being resuspended in RPMI-1640 media. Peripheral blood mononuclear cells (PBMCs) from healthy donors were isolated by density gradient centrifugation with Ficoll-Paque Plus (Cytiva, Sweden). CD3-positive T-cells were isolated from PBMCs using a CD3 T-cell isolation kit (BioLegend) and activated using T-cell activation beads (Thermo Fisher Scientific). Activated T-cells were cultured at a concentration of 1×10^6 cells·mL⁻¹ in RPMI-1640 media supplemented with 10% FBS, 100 IU·mL⁻¹ humanized interleukin-2 (hIL-2), 1% gluta-MAX (Thermo Fisher Scientific), 100 U·mL⁻¹ penicillin G, and 100 µg·mL⁻¹ streptomycin. After 24 h, activated T-cells (0.5×10^6 cells·well⁻¹) were infected with lentivirus in RPMI-1640 medium supplemented with 8 µg·mL⁻¹ polybrene and 100 IU·mL⁻¹ hIL-2 under centrifugation (1000g, 1.5 h, 33 °C). The cells were expanded in fresh IL-2-containing medium for 7 d before use or cryopreservation. All individuals provided informed consent to participate in this study, and approval was provided by the Medical Research Ethics Committee of Peking University Health Science Center (approval No. 2024188).

2.8. Quantification of specific lysis of B lymphoma cells via LDH release assay

NK-92MI cells or T-cells and CD19-CAR-T cells were mixed with different types of cancer cells at the indicated effector/target cell (E/T) ratios for 4–8 h in a 96-well plate. Specific cancer cell lysis was detected by LDH secretion in the supernatant. Specific lysis of target cells was performed according to the manufacturer's instructions.

2.9. Quantification of the formation of cell–cell conjugates via flow cytometry

Lymphoma and engineered immune cells were washed twice with PBS and then incubated in RPMI-1640 with Celltracker Deep Red or Celltracker CMFDA for 30 min at 37 °C. After staining, the cells were mixed at various E/T ratios for 1 h at 37 °C and directly analyzed by flow cytometry using an Attune NxT flow cytometer (Thermo Fisher Scientific). The double-positive signals indicate the formation of cell–cell conjugates. Quantification was performed by calculating the percentage of double-positive (CMFDA⁺/Deep Red⁺) cells relative to the total number of Deep Red⁺ target cells.

2.10. Western blot

Azide-labeled proteins were precipitated with methanol/chloroform and resuspended in 50 µL of PBS containing 1% SDS per 200 µg of protein. Fifty microliter suspensions were incubated with 50 µmol·L⁻¹ CuSO₄-2-(4-((bis((1-(tert-butyl)-1H-1,2,3-triazol-4-yl)methyl)amino)methyl)-1H-1,2,3-triazol-1-yl)acetic acid (BTAA) premixed complex (1:2 mole ratio), 100 µmol·L⁻¹ alkyne-PEG₄-biotin, and 2.5 mmol·L⁻¹ fresh sodium ascorbate at 37 °C for 2 h to perform the click reaction. The samples were resolved by 10% SDS–polyacrylamide gel electrophoresis (PAGE) and imaged by ChemiDoc (Bio-Rad, USA). Biotin was detected using an antibody (1:1000; Cell Signaling Technology), and actin (1:5000; Abcam) was used as a control. Anti-rabbit IgG-HRP (1:5000; ABclonal, China) was used for secondary detection.

2.11. In-gel fluorescence assay

For protein samples, azide-labeled proteins were precipitated with methanol/chloroform and resuspended in 40 µL of PBS containing 1% SDS per 200 µg of protein. Fifty microliter suspensions

were incubated with 50 µmol·L⁻¹ CuSO₄-BTAA premixed complex (1:2 mole ratio), 100 µmol·L⁻¹ alkyne-PEG₄-Cy5, and 2.5 mmol·L⁻¹ fresh sodium ascorbate at 37 °C for 2 h to perform the click reaction. The samples were resolved by 10% SDS–PAGE and imaged with ChemiDoc. The gels were then stained with Coomassie brilliant blue (CBB).

2.12. Tumor models

Male NOD.Cg-Prkdc^{scid} IL2rgtm^{1Wjl}/SzJ (NSG) mice (8–10 weeks old) were inoculated with 1×10^6 Raji-Luc cells through tail vein injection (Day 0). On Day 2, the mice were randomly divided into four groups and treated with HBSS, NK-92MI, ^{MPB}Neu5Ac-modified NK-92MI, or ^{MPB}Neu5Ac/sialyl Lewis X (sLe^x) dual-labeled NK-92MI cells through tail vein injection (7×10^6 NK-92MI cells per mouse). On Day 5 after tumor challenge, the mice were injected with 200 µL of D-luciferin (15 mg·mL⁻¹) through intraperitoneal (i.p.) injection. After 10 min, the bioluminescence signal was measured using an IVIS Lumina Series III (PerkinElmer, USA). The total number of photons indicating the tumor was quantified with IVIS software. To follow the progression of B lymphoma, NSG mice received three additional doses of NK-92MI cells on Days 6, 10, and 14. Luciferin-assisted IVIS monitoring of tumor growth was performed on Days 5, 8, 11, and 13. NSG mice were purchased from Biocytongen Pharmaceuticals (China). All animal study procedures were approved by the Institutional Animal Care and Use Committee of Peking University Health Science Center and performed in accordance with ethical standards (No. DLASBD0224).

3. Results and discussion

3.1. The glycan repertoire defines the engineering efficiency of CeGE vs MGE

In addition to the lipid anchor-assisted incorporation of glycoconjugates, the outermost glycocalyx of live cells provides viable scaffolds for loading functional agents to influence their cellular properties. To date, two major glycan-centric strategies for the functional engineering of live cells, MGE and CeGE, have been intensively evaluated in this field. MGE strategies, which rely on intracellular glycosylation machinery to incorporate small functionalities onto the glycocalyx, have a limited tolerance for substrate modifications. As previously documented, MGE of sialylated glycans using unnatural sugar building blocks (e.g., azide-modified analogs of Sia or N-acetylmannosamine) has robust efficiency. In contrast, CeGE approaches exhibit excellent biocompatibility and broad substrate scope, and their engineering efficiency is largely determined by the membrane content of tunable glycan moieties. Accordingly, we first compared the efficiency of MGE-based sialoside engineering of NK-92MI cells with that of ST6Gal1-assisted CeGE engineering (Fig. 1(a)). The analog of Sia (e.g., the azide derivative Neu5Az) had insufficient plasma membrane penetration, we thus assessed the labeling of NK-92MI cells by 1,6Pr₂ManNAz, a recently developed probe. The dose-dependent incorporation of azides onto NK-92MI cells was probed by conjugation with DBCO–biotin, followed by streptavidin–Alexa Fluor 647 staining and flow cytometry quantification (Fig. 1(b)). As expected, the ST6Gal1-based addition of Neu5Az onto NK-92MI cells was concentration dependent (Fig. 1(c)). The antibiotin western blot results revealed that the intensity of ST6Gal1 labeling was significantly greater than that resulting from metabolic labeling using 1,6Pr₂ManNAz or the previous well-established Ac₄ManNAz under saturated conditions (Figs. 1(d) and (e)).

3.2. Different glycoprotein networks control downstream cellular signaling beyond functionalization

Next, we conducted a comparative glycoproteomic analysis to identify the molecules underlying the differential labeling efficiency, given that the MGE and CeGE approaches involve distinct mechanisms. Following engineering and biotin conjugation, the modified glycoproteins were enriched with avidin-agarose beads for trypsin digestion and subsequent mass spectrometry analysis (Fig. 2(a)). In the ST6Gal1-CeGE group, we confidently identified a total of 463 membrane-associated glycoproteins, which was 2.5-fold greater than that documented in the MGE group (with 184 targets). Compared with that of the MGE approach, the ST6Gal1-assisted CeGE approach covered a significantly greater diversity of glycoproteins (i.e., 344 unique targets), with 119 proteins shared by both types of glycocalyx engineering (Fig. 2(b)). The shared subgroup of proteins accounted for 81.8% of the total

protein intensity in the MGE group versus 46.4% in the CeGE group (Fig. 2(c)), suggesting that the CeGE group exhibited a distinctive glycoproteome.

Notably, the top 40 glycoproteins ranked by normalized abundance included key regulators associated with immune cytotoxicity and adhesion: CD44, CD45, CD47, lymphotactin (XCL1), dipeptidyl peptidase 4 (DPP4), and cadherin 17 (CDH17) (Fig. 2(d), Figs. S1(a) and (b) in Appendix A) [35–40]. GO and KEGG functional enrichment analyses revealed that the shared proteins were involved in NK cell-mediated cytotoxicity and cell adhesion pathways (Fig. 2(e), Fig. S1(c) in Appendix A). Interestingly, the ST6Gal1-CeGE method uniquely modified critical proteins involved in immune synapse formation and NK activation, including CD2, 3-phosphoinositide-dependent protein kinase 1 (PDKP1), Nck-associated protein 1-like (NCKAP1L), signaling lymphocyte activation molecule (SLAM) family receptors (e.g., SLAMF1), and Src family kinases (e.g., LCK) [41–45]. These findings suggest that

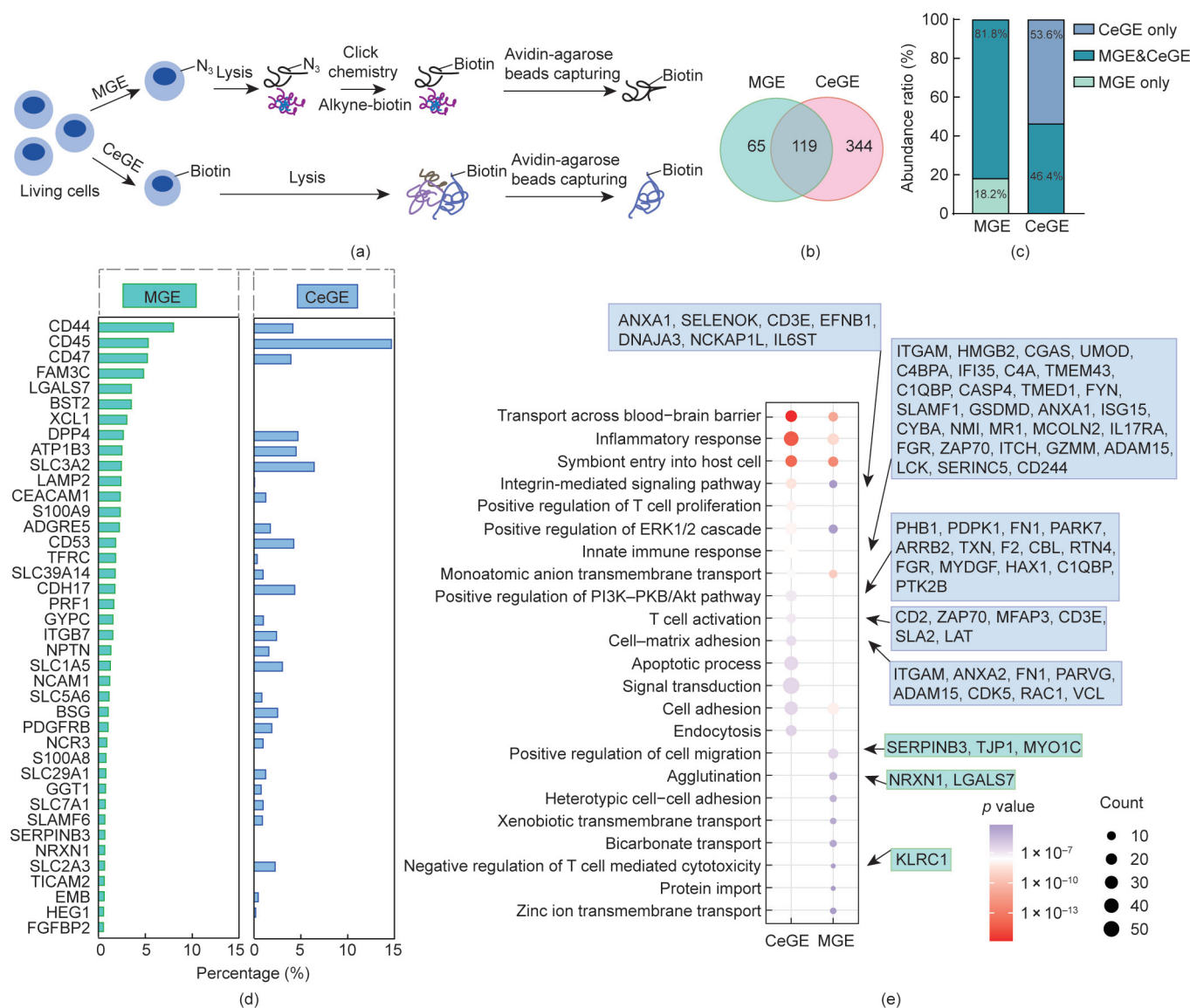


Fig. 2. Comparison of the NK-92MI glycoprotein profiles accessible by MGE and CeGE. (a) Schematic workflow of chemical glycoproteome profiling by mass spectrometry. (b) Venn diagram comparison of membrane glycoproteins modified by CeGE vs MGE. (c) Stack bar chart showing the relative abundance of membrane glycoproteins modified by MGE and CeGE. (d) Rank-ordered abundance profiles of the top 40 membrane glycoproteins accessible by MGE, with parallel quantification in the ST6Gal1-CeGE group. (e) Enriched GO terms of glycoproteins labeled by MGE and CeGE. The colored boxes indicate glycoproteins uniquely identified by each method (green: MGE specific; blue: CeGE specific).

glycoengineering may attach functionalities to glycoproteins critical for NK cell effector functions. After ST6Gal1-CeGE treatment, the selective enrichment of agents (i.e., CD22-target glycan ligands) to immune synapse components may spatially facilitate the formation of cytotoxic machinery at the effector–target interface. Together, the broader glycoprotein coverage and preferential labeling of cytotoxic effectors by ST6Gal1-CeGE make it the preferred method for improving NK cell therapies with CD22-targeting capability.

3.3. Chemoenzymatic incorporation of ^{MPB}Neu5Ac promotes the targeting of B lymphoma cells by NK-92MI cells

Inspired by these mechanistic insights, we explored the feasibility of modifying NK-92MI cells with ^{MPB}Neu5Ac to target CD22 through ST6Gal1-assisted CeGE (Fig. 3(a)). Compared with those of ^{BPC}Neu5Ac, ^{MPB}Neu5Ac has comparable avidity for CD22 but minimal potential off-target side effects because of its negligible affinity for other Siglecs [12]. NK-92MI cells were subsequently treated with ST6Gal1 and CMP-^{MPB}Neu5Ac. The successful chemoenzymatic incorporation of ^{MPB}Neu5Ac onto NK-92MI cells significantly strengthened their binding to CD22 (Fig. 3(b)). Interestingly, compared with that of cells treated with ^{MPB}Neu5Ac-MGE, NK-92MI cells treated with ST6Gal1 for the incorporation of ^{MPB}Neu5Ac demonstrated an approximately 5-fold increase in the avidity of CD22 under saturated conditions (Fig. 3(c)). In addition, neither the MGE- nor the CeGE-mediated installation of ^{MPB}Neu5Ac for CD22 targeting affected the viability or proliferation of NK-92MI cells, suggesting their biocompatibility (Figs. S2(a) and (b) in Appendix A). To assess the ability of ^{MPB}Neu5Ac-modified NK-92MI cells to target cancer cells, we cocultured CMFDA-labeled NK-92MI cells with Deep Red-labeled lymphoma cells (i.e., Ramos, Daudi, Raji, and BJAB cells). The formation of effector–target “cell–cell” conjugates was quantified by flow cytometry (Fig. 3(d), Figs. S2(c) and (d) in Appendix A). The results indicated that ^{MPB}Neu5Ac-NK-92MI cells improved the specific targeting of CD22-positive B lymphoma cells but did not affect binding to CD22-negative Jurkat cells (Fig. 3(e)). Consistent with the findings of Hong et al. [17] using ^{BPC}Neu5Ac-modified NK-92MI cells, ^{MPB}Neu5Ac-modified NK-92MI cells exhibited enhanced cytotoxicity against CD22-positive lymphomas without damaging normal cells (i.e., GM12878 B lymphocytes and PBMCs), as measured by an LDH release assay and flow cytometry (Figs. 3(f)–(i), Figs. S2(e)–(h) in Appendix A). To assess ligand dependence, we prepared corresponding high-affinity ligands on ^{MPB}Neu5Ac-armed NK-92MI cells by α 2,6-linking ^{MPB}Neu5Ac onto *N*-acetylglucosamine (LacNAc) as previously reported [46]. As expected, the better CD22 ligand-mediated lysis of B lymphoma cells was specifically blocked by the addition of ^{MPB}Neu5Ac-LacNAc but not free ^{MPB}Neu5Ac (Fig. S3(a) in Appendix A). In addition to CD22-negative target cells (i.e., Jurkat cells), we further evaluated CD22 dependence by pretreating target B lymphoma cells (i.e., BJAB cells) with CD22-specific blocking antibodies. We observed that the presence of antibodies significantly inhibited the specific lysis of B lymphoma cells by ^{MPB}Neu5Ac-NK-92MI cells, suggesting that CD22 antigens on B lymphoma cells can be targeted by ligands (Fig. S3(b) in Appendix A). These data demonstrated that ST6Gal1-assisted CeGE effectively incorporated ^{MPB}Neu5Ac onto NK-92MI cells to generate CD22-specific high-affinity ligands, thereby enhancing their interaction with and specific lysis of CD22-positive B lymphoma cells. Moreover, improved *in vitro* B lymphoma eradication was achieved using primary NK cells after ST6Gal1-mediated incorporation of ^{MPB}Neu5Ac to generate CD22-high-affinity ligands (Fig. S3(c) in Appendix A), supporting the feasibility of engineering allogenic NK cells for B lymphoma treatment.

3.4. Orthogonal CeGE modifications for the eradication of B lymphoma in a murine model

Owing to the greater selectivity of ^{MPB}Neu5Ac for CD22 compared with that of ^{BPC}Neu5Ac, we evaluated the *in vivo* antitumor efficacy of ^{MPB}Neu5Ac-NK-92MI cells. Effective tumor clearance by NK-92MI cells relies on both their ability to target CD22 and their ability to infiltrate tumors. Adhesion factors, such as E-selectin on vascular endothelial cells, bind to their ligand sLe^X (Neu5Ac α 2,3Gal β 1,4(Fuc α 1,3)GlcNAc) and facilitate the migration of leukocytes to bone marrow and inflamed cancer tissues [47]. Scientists previously demonstrated that the increased expression of sLe^X by human fucosyltransferase VI (hFUT6) is essential for the *in vivo* anti-B lymphoma potency of ^{BPC}Neu5Ac-armed NK-92MI cells [16]. Therefore, we treated ^{MPB}Neu5Ac-modified NK-92MI cells with hFUT6 and its substrate GDP-Fuc. The exogenously added α 1,3-Fuc was stained with AAL, and the strong staining of hFUT6-treated cells relative to that of control cells confirmed the success of α 1,3-fucosylation (Fig. 4(a)). Notably, the application of hFUT6, which added α 1,3-Fuc to NK-92MI cells, resulted in a significant increase in the level of sLe^X, as clearly detected by anti-sLe^X antibody staining, which revealed an approximately 20-fold increase in sLe^X staining of α 1,3-fucosylated NK-92MI cells compared with that of untreated cells (Fig. 4(b)). Moreover, the CD22-Fc binding efficacy of α 1,3-fucosylated NK-92MI cells was comparable to that of ^{MPB}Neu5Ac-NK-92MI cells, highlighting the orthogonality of CD22 ligands generated by ST6Gal1 and sLe^X moieties generated by hFUT6 (Fig. 4(c)).

Next, we evaluated the therapeutic efficacy of ^{MPB}Neu5Ac-NK-92MI cells using a murine model of Raji B lymphoma. On Day 0, Raji-Luc cells, a B lymphoma cell line that constantly expresses firefly luciferase and the tdTomato we developed, were intravenously (i.v.) xenografted into NSG mice. Subsequently, the mice received four rounds of NK-92MI cell treatments (i.v.) on Days 2, 6, 10, and 14 after tumor inoculation (Fig. 4(d)). Bioluminescence imaging was performed on Days 5, 8, 11, and 13. The images clearly revealed that compared with the HBSS control group, the group treated with α 1,3-fucosylated ^{MPB}Neu5Ac-NK-92MI cells had better tumor growth control after Day 11 (Figs. 4(e) and (f)). However, no significant differences were observed between the groups treated with NK-92MI or ^{MPB}Neu5Ac-NK-92MI cells and the HBSS control group. At the terminal stage on Day 17, peripheral blood mononuclear cell analysis confirmed a lower tumor burden only in mice treated with α 1,3-fucosylated ^{MPB}Neu5Ac-modified NK-92MI cells (Fig. 4(g)), which further aligned with the survival statistics, indicating a therapeutic effect in this group (Fig. 4(h)). Together with the results of a previous study on ^{BPC}Neu5Ac-NK-92MI therapeutics, these results highlight the potential of dual orthogonal glycoengineering—targeting both CD22 and selectins—to increase the antitumor efficacy of NK-92MI cells, which is indispensable for improving the survival of tumor-inoculated mice.

3.5. ^{MPB}Neu5Ac modification targeted CD19-CAR-T cells to kill B-cells in lymphoma

Inspired by the improved targeting of CD22-positive B lymphoma by ^{MPB}Neu5Ac-armed NK cells, we explored whether ^{MPB}Neu5Ac could improve CD19-CAR-T therapy. Previous success with multiple-antigen targeting strategies suggests that this approach can effectively address antigen escape and reduce the on-target/off-tumor side effects associated with CD19-CAR-T treatment [9,48]. We hypothesized that the addition of ^{MPB}Neu5Ac could offer a versatile solution. We constructed CD19-CAR-T cells and validated their cytotoxic activity against B-cell lymphomas (Fig. S4 in Appendix A). We then quantified the CD19 antigens

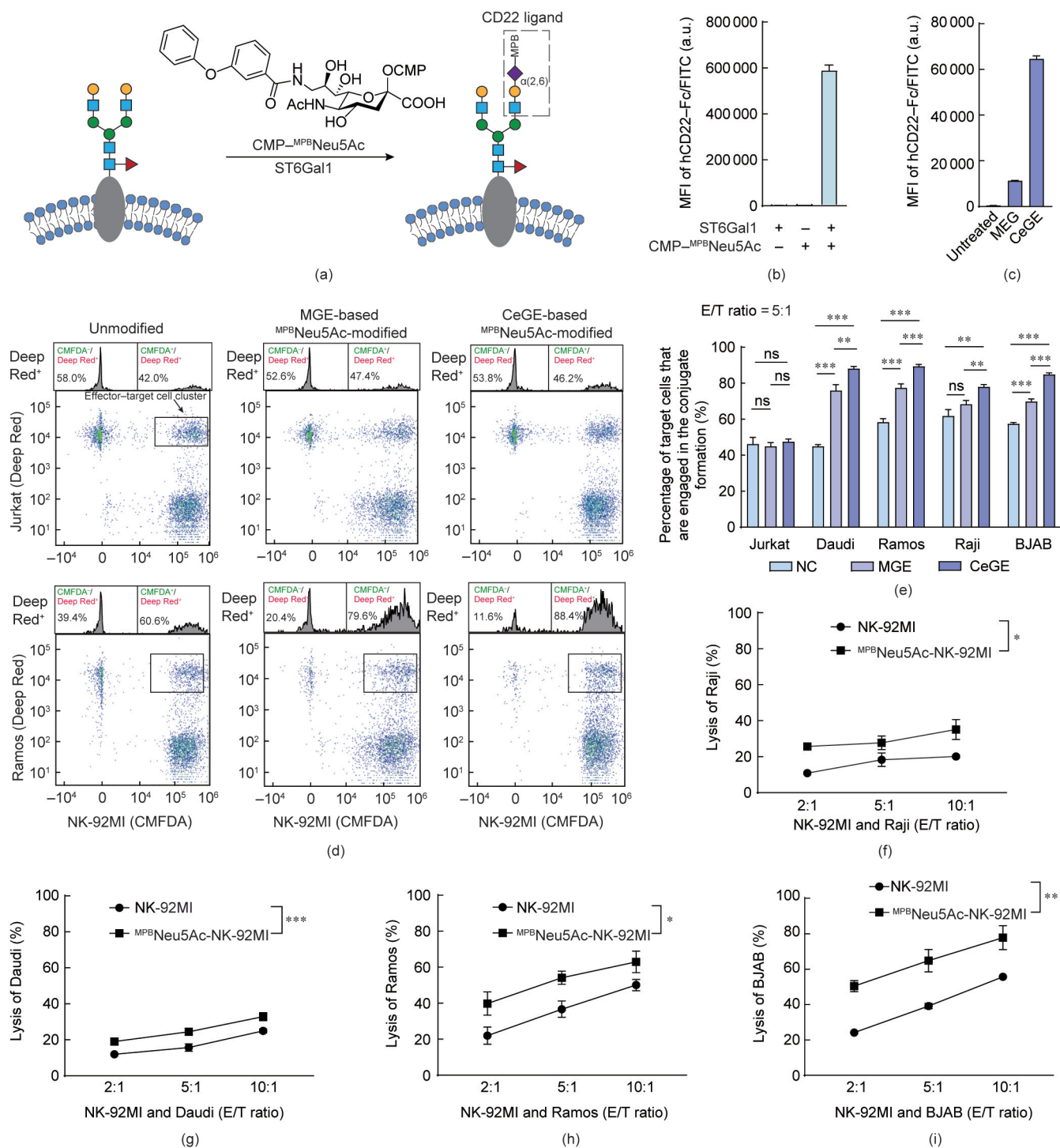


Fig. 3. ^{MPB}Neu5Ac modification enables NK-92MI cells to target B lymphoma. (a) Workflow of the incorporation of ^{MPB}Neu5Ac onto NK-92MI cells via ST6Gal1-assisted CeGE. (b) Flow cytometry quantification of CD22-Fc binding to CeGE-treated NK-92MI cells. (c) Comparison of the CD22 binding efficiency of ^{MPB}Neu5Ac-armed NK-92MI cells by CeGE and MGE approaches using flow cytometry. (d) Flow cytometry-based detection of cell-cell conjugates of NK-92MI (effector cells, stained with CMFDA) and target cells (Ramos or Jurkat cells, stained with Deep Red) at an E/T ratio of 5:1. Adjunct histograms were used to quantify the effector-target cell conjugates by comparing CMFDA-positive and CMFDA-negative cells in the target cell population (Deep Red-positive cells). (e) Quantification of the formation of the NK-92MI-target cell conjugate. (f–i) LDH release assay-based quantification of NK-92MI cytotoxicity against (f) Raji, (g) Daudi, (h) Ramos, and (i) BJAB cells. The error bars in the figures represent the mean ± s.d., n = 3. For (e), statistical significance was assessed using a two-sided Student's *t* test. For (f)–(i), statistical analyses were conducted using two-way ANOVA. **p* < 0.05, ***p* < 0.01, ****p* < 0.001, ns: not significant.

present on CD22-positive B lymphoma cell lines, including BJAB, Ramos, and Daudi, using Jurkat cells as CD19-negative controls (Fig. S4(c)). Dose-dependent incorporation of Neu5Az through ST6Gal1-assisted engineering confirmed a tunable glycan subset

on CD19-CAR-T cells (Fig. 5(a)). The ST6Gal1-mediated addition of ^{MPB}Neu5Ac enhanced the binding of CD19-CAR-T cells, despite the loading efficiency not being as pronounced as that observed in NK-92MI cells (Figs. 3(b) and 5(b)). This difference may be due

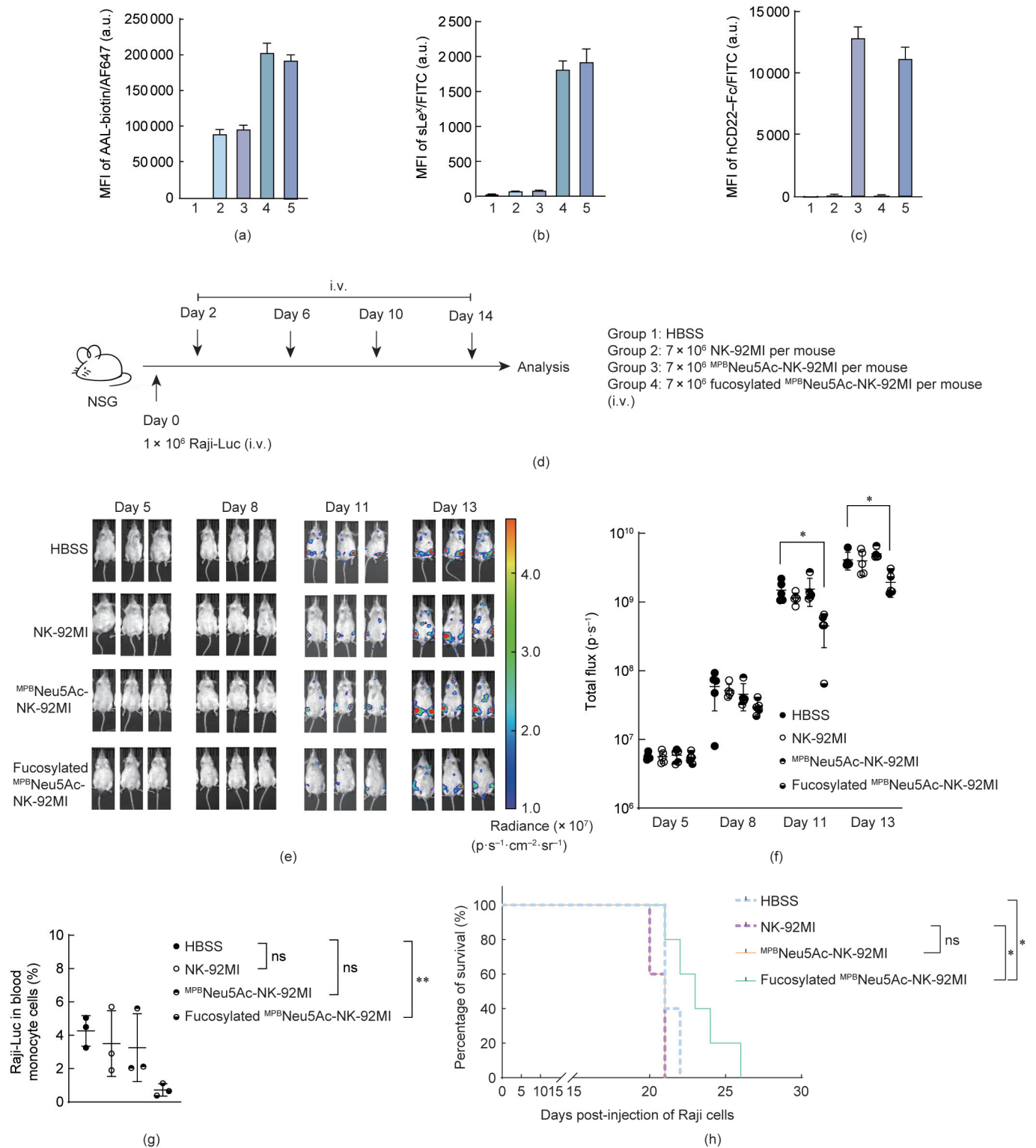


Fig. 4. Suppression of B lymphoma growth by ^{MPB}Neu5Ac-armed NK-92MI cells in a murine xenograft model. (a–c) Sequential glycoengineering of NK-92MI cells: ST6Gal1-mediated ^{MPB}Neu5Ac conjugation followed by FUT6-catalyzed α 1-3-fucosylation to generate sLe^x. The cell-surface creation of α 1,3-fucosides, sLe^x, and CD22-ligands was confirmed by flow cytometry using (a) AAL-biotin, (b) anti-sLe^x antibody, and (c) CD22-Fc staining, respectively. (d) Workflow for the adoptive transfer of ^{MPB}Neu5Ac-NK-92MI cells with or without sLe^x to B lymphoma-bearing NSG mice. (e) *In vivo* bioluminescence imaging (IVIS) of Raji-Luc leukemic burden at the indicated time points in mice injected with *D*-luciferin. (f) Quantification of the total flux of the Raji-Luc leukemic burden measured by the IVIS system. (g) Flow cytometry analysis of circulating Raji cells in B lymphoma-bearing mice at the terminal stages of tumor progression. (h) Kaplan–Meier survival curves for mice treated with NK-92MI cell therapy. Five mice per treatment group are shown. The error bars in the figures represent the mean \pm s.d., $n = 3$. Two-sided Student's *t* test. * $p < 0.05$, ** $p < 0.01$, ns: not significant. In (a–c), 1: w/o staining, 2: NK-92MI, 3: ^{MPB}Neu5Ac-NK-92MI, 4: α 1,3-fucosylated NK-92MI, 5: α 1,3-fucosylated ^{MPB}Neu5Ac-NK-92MI. p·s⁻¹: photon per second.

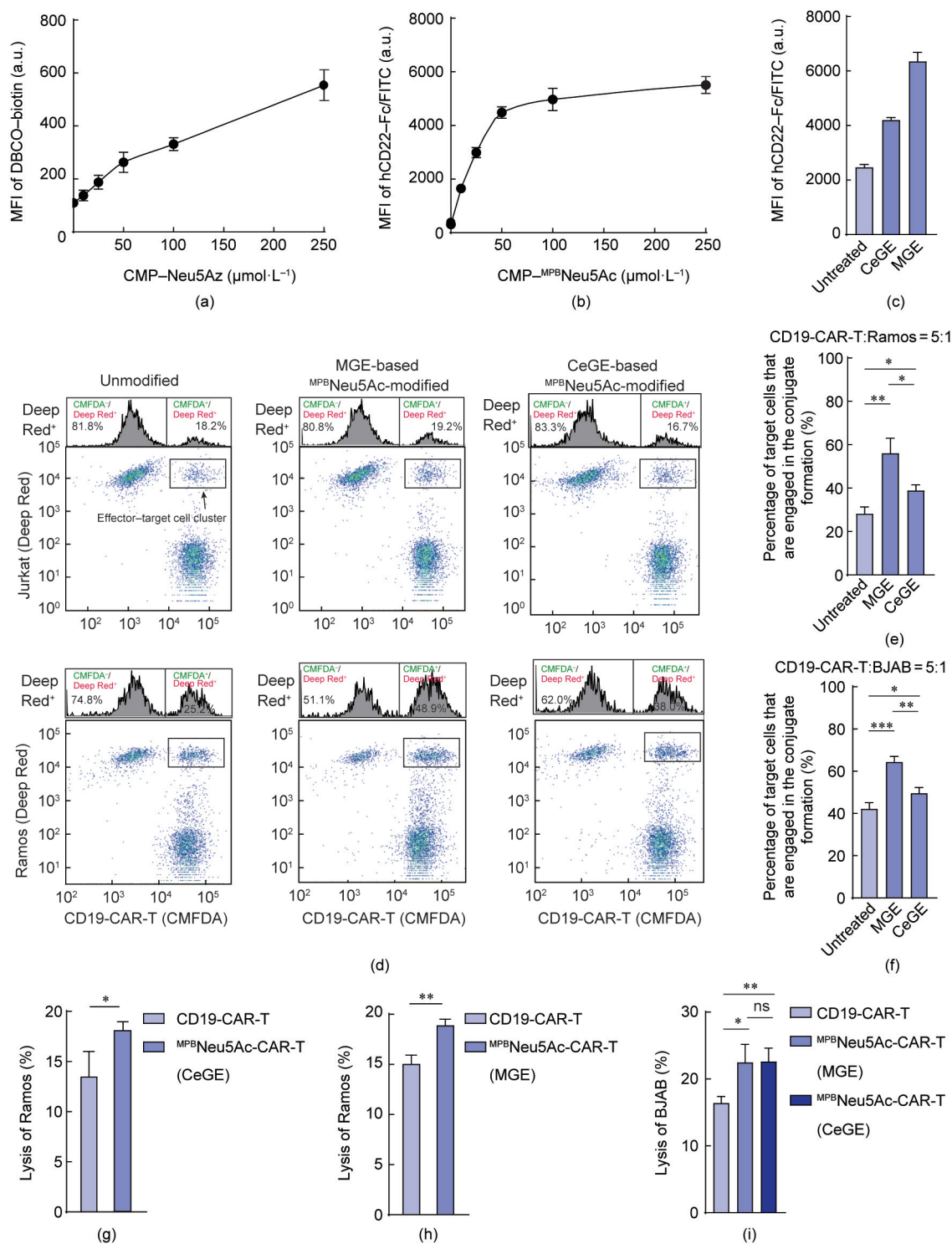


Fig. 5. ^{MPB}Neu5Ac modification promotes the targeting of B lymphoma by CD19-CAR-T cells. (a) Quantification of the ST6Gal1-assisted CeGE labeling of NK-92MI cells by flow cytometry. (b) Flow cytometry quantification of CD22 binding on CeGE-assisted ^{MPB}Neu5Ac-modified CD19-CAR-T cells. (c) Comparison of the CD22 binding efficiency between ^{MPB}Neu5Ac-armed CD19-CAR-T cells by CeGE and MGE approaches using flow cytometry. (d) Formation of cell–cell conjugates between CMFDA-labeled CD19-CAR-T effector cells and Deep Red-labeled target cells (Ramos or Jurkat) at an E/T ratio of 5:1, as measured by flow cytometry. Adjunct histograms were used to quantify the effector–target cell conjugates by comparing CMFDA-positive and CMFDA-negative cells in the target cell population (Deep Red-positive cells). (e, f) Quantification of the formation of conjugates between CD19-CAR-T cells and the B lymphoma cell lines (e) Ramos and (f) BJAB. (g, h) LDH release assay-based quantification of (g) CeGE- and (h) MGE-assisted ^{MPB}Neu5Ac-CD19-CAR-T cytotoxicity against Ramos cells. (i) Comparison of the cytotoxicity efficiency of CeGE- and MGE-assisted ^{MPB}Neu5Ac-CD19-CAR-T cells against BJAB cells using an LDH release assay. The error bars in the figures represent the mean \pm s.d., $n = 3$. Two-sided Student's t test. * $p < 0.05$. ** $p < 0.01$. *** $p < 0.001$. ns: not significant.

to the significantly higher sialylation levels on CAR-T cells relative to NK cells, which results in fewer available scaffolds for Sia modification. This speculation was supported by staining with SNA

(specific for α 2,6-linked Sia) and MAL-II (specific for α 2,3-linked Sia), which revealed high levels of both α 2,3- and α 2,6-linked Sia residues on CAR-T cells (Fig. S5(a) in Appendix A). Moreover, we

observed donor-dependent variability in labeling efficacy, suggesting differences in glycoengineering outcomes among donors (Fig. S5(b) in Appendix A). Given the high levels of surface sialylation on CAR-T cells, we compared the ^{MPB}Neu5Ac engineering efficiency between ST6Gal1-CeGE and ^{MPB}Neu5Ac-MGE for CAR-T cell modification. CD22-Fc staining revealed marginally superior modification efficiency with MGE versus CeGE (Fig. 5(c)).

We subsequently assessed the formation of cell–cell conjugates between CAR-T cells and cancer cells by coculturing CMFDA-labeled CAR-T cells with Deep Red-labeled lymphoma cells. ^{MPB}Neu5Ac modification significantly increased the binding of CD19-CAR-T cells to CD22-positive Ramos cells but did not improve the binding of CD22-negative Jurkat cells (Fig. 5(d), Fig. S5(c) in Appendix A). Expanded testing across different donors and tumor lines confirmed increased targeting of CD22-expressing malignancies, despite variation in the efficacy among CD22-positive tumors (Figs. 5(e) and (f), Fig. S5(d) in Appendix A). Moreover, ^{MPB}Neu5Ac-CD19-CAR-T cells exhibited enhanced cytotoxicity against CD22/CD19-positive lymphoma cells (Figs. 5(g)–(i)). No significant difference in cytotoxic efficacy was found between CeGE- and MGE-engineered CAR-T cells. This finding may be attributed to the efficient formation of immune synapses associated with CeGE engineering. Collectively, these results demonstrate that ^{MPB}Neu5Ac ligands on engineered CD19-CAR-T cells improve their ability to recognize and kill multiple types of CD22-positive B lymphoma cells; however, the potential of using CD22-ligand-armed CD19-CAR-T cells to mitigate antigen escape needs further *in vivo* exploration.

4. Conclusions

It is well established that glycosylation in the secretory pathway defines the molecular repertoire of the surface glycocalyx on live cells by linking carbohydrate moieties to proteins and lipids. Recently, the discovery of RNA N-glycosylation has complicated these cell-surface molecular networks, in addition to inspiring concerns about DNA glycosylation [49,50]. Owing to their remarkable structure-to-information coding divergence, recognized as the third alphabet of life, abnormal glycans play vital (patho)physiological roles in diseases such as cancers and neurodegenerative diseases [26]. Characterizing glycan fingerprints with high-throughput omics has thus empowered the discovery of markers on glycoconjugates and live cells to differentiate health and disease [51,52]. These outermost scaffolds present ideal frames to load functionalities, and live-cell glycocalyx engineering has emerged as a highly compatible and flexible means for loading agents to endow cellular immunotherapies with desired functions, such as via MGE and CeGE. In the current study, we compared the labeling efficiency and molecular characteristics of 1,6Pr₂ManNAz-assisted MGE and ST6Gal1-assisted CeGE in NK-92MI cells. ST6Gal1-CeGE exhibited comparable or even superior ligand-loading efficiency (about 2.5-fold), with many immune synapse components (e.g., LCK and SLAMF1) modified, which may improve the spatial recognition of target cells. The superiority of ST6Gal1-assisted CeGE compared with the MGE approach for functionalization of immune cells (i.e., NK-92MI cells, primary NK cells, and CD19-CAR-T cells) to treat B lymphoma was elucidated and expanded. CeGE-assisted CD22-specific ^{MPB}Neu5Ac-NK-92MI cells exhibited superior targeting and cytotoxicity against B lymphoma *in vitro*, and fucosylated ^{MPB}Neu5Ac-NK-92MI cells showed significant antitumor efficacy *in vivo*. In addition to addressing the potential off-target effects of CD19-CAR-T-cell therapy in clinical settings, MGE- and ST6Gal1-mediated CeGE glycocalyx engineering were applied to incorporate ^{MPB}Neu5Ac onto CD19-CAR-T cells. The *in situ* generation of CD22-specific high-affinity ligands on CD19-

CAR-T cells facilitated their lysis of CD19/CD22 B lymphoma cells in a cell coculture assay. Compared with cost-effective MGE, which relies on intracellular glycosylation machinery to incorporate ligands, culture-free CeGE engineering is time-saving and easy to transfer in many settings (e.g., engineering of live cell-free cellular derivatives). Notably, the elimination of multiple target cells by ^{MPB}Neu5Ac-NK-92MI cells significantly increased when B lymphoma and effector cells were cocultured. However, no substantial *in vivo* tumor eradication was observed unless ^{MPB}Neu5Ac-modified effector NK-92MI cells were also modified by hFUT6 to add α1,3-Fuc, which acts as an E-selectin ligand to guide them to tumor sites. For clinical applications, our proof-of-concept studies still require in-depth assessment for such synergistic treatment (e.g., *in vivo* evaluations). Additionally, ^{MPB}Neu5Ac exhibits limited avidity for CD22, and more substantial benefits may be achieved by other high-avidity structures [11]. This study is expected to stimulate interest in the preparation of novel glycoligand-armed immunotherapies via glycocalyx engineering, thus revealing their potential to improve B lymphoma treatment. This could be helpful in meeting the growing demand for the nongenetic engineering of immune cells that exhibit high compatibility. The glycoproteomic profile provides fundamental information for immune cell engineering, and CeGE offers ideal tools for functionalizing immune cells for clinical applications.

CRedit authorship contribution statement

Yuxin Li: Writing – review & editing, Writing – original draft, Formal analysis, Data curation, Conceptualization. **Tao Gao:** Writing – original draft, Methodology, Formal analysis, Data curation. **Zhaoxin Han:** Data curation. **Valeria M. Stepanova:** Resources. **Han Wang:** Data curation. **Hongmin Chen:** Data curation. **Alexey Stepanov:** Supervision, Resources. **Senlian Hong:** Writing – review & editing, Writing – original draft, Supervision, Funding acquisition, Conceptualization.

Declaration of competing interest

The authors declare that they have no known competing financial interests or personal relationships that could have appeared to influence the work reported in this paper.

Acknowledgments

We gratefully acknowledge the financial support from the National Natural Science Foundation of China (32150027 and 22177002) and the National Key Research and Development Program of China (2022YFC3400803 and 2023YFC2308003). Valeria M. Stepanova and Alexey Stepanov were partially supported by the Russian Science Foundation (5-74-30002).

Appendix A. Supplementary data

Supplementary data to this article can be found online at <https://doi.org/10.1016/j.eng.2025.08.037>.

References

- [1] Cappell KM, Kochenderfer JN. Long-term outcomes following CAR T cell therapy: what we know so far. *Nat Rev Clin Oncol* 2023;20(6):359–71.
- [2] Stepanova VM, Volkov DV, Osipova DS, Wang W, Hou Y, Pershin DE, et al. Targeting CD45 by gene-edited CAR T cells for leukemia eradication and hematopoietic stem cell transplantation preconditioning. *Mol Ther Oncol* 2024;32(3):200843.
- [3] Saez-Ibañez AR, Upadhya S, Partridge T, Shah M, Correa D, Campbell J. Landscape of cancer cell therapies: trends and real-world data. *Nat Rev Drug Discov* 2022;21(9):631–2.

- [4] Vivier E, Rebuffet L, Narni-Mancinelli E, Cornen S, Igarashi RY, Fantin VR. Natural killer cell therapies. *Nature* 2024;626(8000):727–36.
- [5] Oliveira G, Wu CJ. Dynamics and specificities of T cells in cancer immunotherapy. *Nat Rev Cancer* 2023;23(5):295–316.
- [6] Bashor CJ, Hilton IB, Bandukwala H, Smith DM, Veiseh O. Engineering the next generation of cell-based therapeutics. *Nat Rev Drug Discov* 2022;21(9):655–75.
- [7] Nitschke L. CD22 and Siglec-G: B-cell inhibitory receptors with distinct functions. *Immunol Rev* 2009;230(1):128–43.
- [8] Shah NN, Sokol L. Targeting CD22 for the treatment of B-cell malignancies. *ImmunoTargets Ther* 2021;10:225–36.
- [9] Frank MJ, Baird JH, Kramer AM, Srinagesh HK, Patel S, Brown AK, et al. CD22-directed CAR T-cell therapy for large B-cell lymphomas progressing after CD19-directed CAR T-cell therapy: a dose-finding phase 1 study. *Lancet* 2024;404(10450):353–63.
- [10] Schneider D, Xiong Y, Wu D, Hu P, Alabanza L, Steimle B, et al. Trispecific CD19–CD20–CD22-targeting duoCAR-T cells eliminate antigen-heterogeneous B cell tumors in preclinical models. *Sci Transl Med* 2021;13(586):eabc6401.
- [11] Büll C, Heise T, Adema GJ, Boltje TJ. Sialic acid mimetics to target the sialic acid–Siglec axis. *Trends Biochem Sci* 2016;41(6):519–31.
- [12] Rillahan CD, Macauley MS, Schwartz E, He Y, McBride R, Arlian BM, et al. Disubstituted sialic acid ligands targeting Siglecs CD33 and CD22 associated with myeloid leukaemias and B cell lymphomas. *Chem Sci* 2014;5(6):2398–406.
- [13] Prescher H, Schweizer A, Frank M, Kuhfeldt E, Ring J, Nitschke L. Targeting human CD22/Siglec-2 with dimeric sialosides as novel oligosaccharide mimetics. *J Med Chem* 2022;65(15):10588–610.
- [14] Hansel TT, Kropshofer H, Singer T, Mitchell JA, George AJ. The safety and side effects of monoclonal antibodies. *Nat Rev Drug Discov* 2010;9(4):325–38.
- [15] Chen WC, Completo GC, Sigal DS, Crocker PR, Saven A, Paulson JC. *In vivo* targeting of B-cell lymphoma with glycan ligands of CD22. *Blood* 2010;115(23):4778–86.
- [16] Wang X, Lang S, Tian Y, Zhang J, Yan X, Fang Z, et al. Glycoengineering of natural killer cells with CD22 ligands for enhanced anticancer immunotherapy. *ACS Cent Sci* 2020;6(3):382–9.
- [17] Hong S, Yu C, Wang P, Shi Y, Cao W, Cheng B, et al. Glycoengineering of NK cells with glycan ligands of CD22 and selectins for B-cell lymphoma therapy. *Angew Chem Int Ed* 2020;60(7):3603–10.
- [18] Wang H, Mooney DJ. Metabolic glycan labelling for cancer-targeted therapy. *Nat Chem* 2020;12(12):1102–14.
- [19] Lam YY, Tan A, Kempe K, Boyd BJ. Metabolic glycan labelling with bio-orthogonal targeting and its potential in drug delivery. *J Control Release* 2025;378:880–98.
- [20] Mondal N, Silva M, Castano AP, Maus MV, Sackstein R. Glycoengineering of chimeric antigen receptor (CAR) T-cells to enforce E-selectin binding. *J Biol Chem* 2019;294(48):18465–74.
- [21] Liu CG, Wang Y, Liu P, Yao QL, Zhou YY, Li CF, et al. Aptamer-T cell targeted therapy for tumor treatment using sugar metabolism and click chemistry. *ACS Chem Biol* 2020;15(6):1554–65.
- [22] Qian H, Fu Y, Guo M, Chen Y, Zhang D, Wei Y, et al. Dual-aptamer-engineered M1 macrophage with enhanced specific targeting and checkpoint blocking for solid-tumor immunotherapy. *Mol Ther* 2022;32(7):2423–4.
- [23] Wang X, Luo X, Tian Y, Wu T, Weng J, Li Z, et al. Equipping natural killer cells with cetuximab through metabolic glycoengineering and bioorthogonal reaction for targeted treatment of KRAS mutant colorectal cancer. *ACS Chem Biol* 2021;16(4):724–30.
- [24] Mo J, Zou Y, Li BH, Li G, Zheng XJ, Liu Y, et al. Tumor-associated extracellular microvesicles with fluorine-modified carbohydrate antigens trigger a stronger antitumor immune response. *ACS Appl Mater Interfaces* 2023;15(34):40201–12.
- [25] Wang B, Liu S, Li H, Dong W, Liu H, Zhang J, et al. Facile preparation of carbohydrate-containing adjuvants based on self-assembling glycopeptide conjugates. *Angew Chem Int Ed* 2024;63(1):e202309140.
- [26] Yang K, Li X, Lai M, Zhao W, Song W, Chen S, et al. Ablation of ST6Gal-I downregulates BACE1 expression and suppresses production of A β 42 plaques in Alzheimer's disease. *Engineering*. In press.
- [27] Sun J, Huang Z, Du Y, Lv P, Fan X, Dai P, et al. Metabolic glycan labeling in primary neurons enabled by unnatural sugars with no S-glyco-modification. *ACS Chem Biol* 2023;18(6):1416–24.
- [28] Peng W, Paulson JC. CD22 ligands on a natural N-glycan scaffold efficiently deliver toxins to B lymphoma cells. *J Am Chem Soc* 2017;139(36):12450–8.
- [29] Cheng B, Wang C, Hao Y, Wang J, Xia X, Zhang H, et al. Facile synthesis of clickable unnatural sugars in the unprotected and 1,6-di-O-acylated forms for metabolic glycan labeling. *Chemistry* 2023;29(11):e202203054.
- [30] Moremen KW, Ramiah A, Stuart M, Steel J, Meng L, Forouhar F, et al. Expression system for structural and functional studies of human glycosylation enzymes. *Nat Chem Biol* 2018;14(2):156–62.
- [31] McDonald WH, Tabb DL, Sadygov RG, MacCoss MJ, Venable J, Graumann J, et al. MS1, MS2, and SQT—three unified, compact, and easily parsed file formats for the storage of shotgun proteomic spectra and identifications. *Rapid Commun Mass Spectrom* 2004;18(18):2162–8.
- [32] Xu T, Venable JD, Park SK, et al. ProLuCID, a fast and sensitive tandem mass spectra-based protein identification program. *Mol Cell Proteomics* 2006;5:s174.
- [33] Peng J, Elias JE, Thoreen CC, Licklider LJ, Gygi SP. Evaluation of multidimensional chromatography coupled with tandem mass spectrometry (LC/LC-MS/MS) for large-scale protein analysis: the yeast proteome. *J Proteome Res* 2003;2(1):43–50.
- [34] Cociorva DL, Tabb D, Yates JR. Validation of tandem mass spectrometry database search results using DTASelect. *Curr Protoc Bioinformatics* 2007;13:13.4.
- [35] Sackstein R, Merzaban JS, Cain DW, Dagia NM, Spencer JA, Lin CP, et al. *Ex vivo* glycan engineering of CD44 programs human multipotent mesenchymal stromal cell trafficking to bone. *Nat Med* 2008;14(2):181–7.
- [36] Hermiston ML, Xu Z, Weiss A. CD45: a critical regulator of signaling thresholds in immune cells. *Annu Rev Immunol* 2003;21(1):107–37.
- [37] Hayat SMG, Bianconi V, Pirro M, Jaafari MR, Hatamipour M, Sahebkar A. CD47: role in the immune system and application to cancer therapy. *Cell Oncol* 2020;43(1):19–30.
- [38] Lei Y, Takahama Y. XCL1 and XCR1 in the immune system. *Microbes Infect* 2012;14(3):262–7.
- [39] Wagner L, Klemann C, Stephan M, von Hörsten S. Unravelling the immunological roles of dipeptidyl peptidase 4 (DPP4) activity and/or structure homologue (DASH) proteins. *Clin Exp Immunol* 2016;184(3):265–83.
- [40] Marshall JF. Targeting CDH17 in cancer: when blocking the ligand beats blocking the receptor? *Clin Cancer Res* 2018;24(2):253–5.
- [41] Stephen LA, ElMaghloob Y, McIlwraith MJ, Yelland T, Castro Sanchez P, Roda-Navarro P, et al. The ciliary machinery is repurposed for T cell immune synapse trafficking of LCK. *Dev Cell* 2018;47(1):122–132.e4.
- [42] Castro CN, Rosenzweig M, Carapito R, Shahrooei M, Konantz M, Khan A, et al. NCKAP1L defects lead to a novel syndrome combining immunodeficiency, lymphoproliferation, and hyperinflammation. *J Exp Med* 2020;217(12):e20192275.
- [43] De Calisto J, Wang N, Wang G, Yigit B, Engel P, Terhorst C. SAP-dependent and -independent regulation of innate T cell development involving SLAMF receptors. *Front Immunol* 2014;5:186.
- [44] Nirula A, Ho M, Phee H, Roose J, Weiss A. Phosphoinositide-dependent kinase 1 targets protein kinase A in a pathway that regulates interleukin 4. *J Exp Med* 2006;203(7):1733–44.
- [45] McNerney ME, Kumar V. The CD2 family of natural killer cell receptors. *Curr Top Microbiol Immunol* 2006;298:91–120.
- [46] Hong S, Shi Y, Wu NC, Grande G, Douthit L, Wang H, et al. Bacterial glycosyltransferase-mediated cell-surface chemoenzymatic glycan modification. *Nat Commun* 2019;10(1):1799.
- [47] Varki A. Selectin ligands. *Proc Natl Acad Sci USA* 1994;91(16):7390–7.
- [48] Spiegel JY, Patel S, Muffly L, Hossain NM, Oak J, Baird JH, et al. CAR T cells with dual targeting of CD19 and CD22 in adult patients with recurrent or refractory B cell malignancies: a phase 1 trial. *Nat Med* 2021;27(8):1419–31.
- [49] Wang, W. Can DNA be glycosylated? *Engineering*. In press.
- [50] Flynn RA, Pedram K, Malaker SA, Batista PJ, Smith BAH, Johnson AG, et al. Small RNAs are modified with N-glycans and displayed on the surface of living cells. *Cell* 2021;184(12):3109–24.e22.
- [51] Zuniga-Banuelos FJ, Hoffmann M, Reichl U, Rapp E. New avenues for human blood plasma biomarker discovery via improved in-depth analysis of the low-abundant N-glycoproteome. *Engineering*. In press.
- [52] Liu X, Meng Y, Fu B, Song H, Gu B, Zhang Y, et al. GlycoPro: a high-throughput sample-processing platform for multi-glycosylation-omics analysis. *Engineering*. In press.